A geostatistical framework for incorporating transport information in estimating the distribution of a groundwater contaminant plume

Shahar Shlomi[1] and Anna M. Michalak[1]

Received 25 April 2006; revised 1 September 2006; accepted 13 October 2006; published 8 March 2007.

[1] The goal of groundwater contaminant plume interpolation is to provide an accurate representation of the spatial distribution of the plume given the data limitations associated with sparse monitoring networks with irregular geometries. Currently available methods for plume estimation cannot fully take advantage of prior knowledge of flow and transport information or the location of a contaminant source. This paper presents two new geostatistical tools for incorporating transport information in estimating the spatial distribution of groundwater contaminant plumes. The methods account for the spatial/temporal covariance of the contaminant plume in defining a best estimate of the plume distribution and its associated uncertainty. Overall, the methods require that the estimated plume distribution be physically feasible given both the available concentration measurements and the flow and transport in the affected aquifer. Sample applications in homogeneous and heterogeneous formations are presented. Even with relatively few observations, the new methods yield results that are superior to those obtained by kriging, with a better reproduction of the true plume shape and lower uncertainty.

Citation: Shlomi, S., and A. M. Michalak (2007), A geostatistical framework for incorporating transport information in estimating the distribution of a groundwater contaminant plume, *Water Resour. Res.*, *43*, W03412, doi:10.1029/2006WR005121.

1. Introduction

[2] Groundwater provides one third of the world's drinking water. Because surface water is largely allocated, demand on the finite groundwater resources is increasing. However, groundwater is highly susceptible to contamination. This vulnerability can limit the value of the resource to society as a whole. Groundwater can be contaminated by localized releases from waste disposal sites, landfills, and underground storage tanks. Pesticides, fertilizers, salt water intrusion, and contaminants from other nonpoint source pollutants are also major sources of groundwater contamination [*Commission on Geosciences, Environment and Resources*, 1993].

[3] In order to avoid, or at least minimize, pumping of polluted groundwater, the extent of any contamination plume has to be known. Because samples can typically only be taken at a few discrete points of a plume (i.e., at wells), they have to be interpolated in order to depict the span of the whole plume. Groundwater contaminant plume interpolation is a difficult task, as contaminant concentration fields are highly heterogeneous, anisotropic, and nonstationary phenomena [*Reed et al.*, 2004].

[4] In addition to concentration measurements, there usually exist other forms of information that can potentially improve interpolation. Often, these secondary data can be spatially and/or temporally correlated with the measured concentrations. These data can enhance the estimation results if used, for example, in a cokriging setup [e.g., *Cassiani and Medina*, 1997]. However, many types of data cannot easily be assimilated into a geostatistical analysis. This category may include information about the physical processes that created the contaminant plume, or a groundwater model that quantitatively describes the flow and transport in the aquifer.

[5] In many environmental applications, data are extremely limited. Therefore the ability to incorporate different forms of data (e.g., physical behavior as expressed in fate-and-transport models and spatial correlation as quantified by geostatistical analyses) would improve the ability to describe the shape and extent of groundwater contaminant plumes. The high cost associated with groundwater monitoring and the high risks posed by these contaminants contribute to the importance of developing a robust plume distribution estimation technique that takes into account diverse types of data for plume interpolation.

2. Currently Available Methods

[6] Plume estimation can be based either on mathematical or statistical manipulation of measured contaminant concentrations, or on the physics of the transport process that created the plume. When concentration measurements are the only data available, interpolation methods such as geostatistical kriging or inverse distance weighted interpolation are typically used. When additional hydrological parameters are available, flow-and-transport models are often employed.

[7] In general, kriging can use measurements at sampled locations, incorporate trends, and take advantage of measurements of certain other related variables (e.g., cokriging).

[1]Department of Civil and Environmental Engineering, University of Michigan, Ann Arbor, Michigan, USA.

0043-1397/07/2006WR005121

Spatial analysis can be performed to identify spatial trends and variogram structures to be used in the estimation process. Thus the variogram or covariance matrix contains additional information, in the form of correlation or variance as a function of distance between points. However, many types of supplementary physical data, such as flow and transport information, cannot be directly used in kriging. *Cooper and Istok* [1988] presented the use of geostatistics to map contaminant concentrations and estimation errors in a groundwater plume, from a set of measured contaminant concentrations. *Reed et al.* [2004] compared two inverse distance weighting techniques and four kriging techniques for plume interpolation. They ultimately concluded that quantile kriging [*Journel and Deutsch*, 1997] was the most robust method for their specific application. They recommended using deterministic methods only as screening tools. *Jones et al.* [2003] compared three different three-dimensional plume interpolation techniques (kriging, natural neighbor, and inverse distance weighted interpolation) and demonstrated that kriging usually results in the lowest error. Geostatistics can also be used to generate stochastic realizations of regionalized variables [*Delhomme*, 1978]. *Boeckenhauer et al.* [2000] used nonparametric regression and kriging to produce regional estimates of groundwater contamination by modeling their data as a realization of a lognormal stochastic process.

[8] Variants and extensions of kriging can be used to introduce additional information into geostatistical analyses. *Diggle et al.* [1998] defined model-based geostatistics by modeling observations as a generalized linear model. *Figueira et al.* [2001] measured the concentration of chloride and sodium in plants, and used three additional factors (the distance from the coast, the intensity of rain observed before the sampling date and the dry period before sampling) in the definition of a space-time trend. *Kitanidis and Shen* [1996] added one parameter to linear geostatistics to account for the skewness of concentration distributions. *Liu* [2003] incorporated gradient or sensitivity information into existing kriging techniques for various multidisciplinary design optimization procedures; the approach treated gradients at the sample points as secondary functions. All of these methods analyzed various aspects of the measured distribution, but they did not consider the source of the contamination or the process of transport.

[9] Several studies have combined the use of kriging/interpolation and groundwater transport models in hydrology. Some have used stochastic [e.g., *Wagner and Gorelick*, 1987] and geostatistical [e.g., *Vyas et al.*, 2004] methods to estimate parameters for flow-and-transport models, or to interpolate input data to these models [e.g., *Feehley et al.*, 2000]. *Saito and Goovaerts* [2001] presented a variant of kriging with a trend for incorporating source location and wind velocity in the interpolation of soil contaminant concentrations. To the knowledge of the authors, however, flow-and-transport models have not themselves been used for the specific purpose of estimating the current distribution of existing groundwater contaminant plumes. This type of use would require knowledge of the boundary conditions, including all contaminant sources and their behavior in space and time. Excluding controlled tracer experiments [e.g., *Mackay et al.*, 1986], this information is generally not available.

[10] Thus the advantage that transport models have to offer, such as information about the physics controlling advection, dispersion, retardation, and chemical behavior, cannot be fully utilized by methods currently available for estimating the distribution of contaminant plumes.

3. Objective

[11] In this paper, we present two new methods for estimating the distribution of groundwater contaminant plumes. Unlike existing tools, these methods take into account both the spatial covariance structure of the concentration field, and available flow and transport information. The concentration data are directly coupled with the transport model to estimate concentrations at unsampled locations. Thus both data pertaining to the autocorrelation of concentrations, and results of a physical flow-and-transport model are assimilated into a common framework.

[12] The first method is referred to as inverse/forward modeling (IFM). It uses an existing transport model for the aquifer and knowledge of the contaminant source location to estimate the time series of the contaminant release into the aquifer and its associated uncertainty. Together with the transport model, this release history is then used to estimate the current plume distribution and its uncertainty.

[13] The second proposed method, transport-enhanced kriging (TREK), combines the merits of IFM with geostatistical kriging, in order to also take advantage of the spatial covariance structure of the available concentration measurements. Thus the resulting predictions are both physically feasible, and exhibit the expected spatial autocorrelation characteristics.

4. Methodology

4.1. Geostatistical Inverse Modeling

[14] The following section outlines the geostatistical approach to inverse modeling, which we implement in this work to estimate the time series of the contaminant release into the aquifer in both of the proposed methods. No derivations are provided, and the reader is referred to, for example, *Kitanidis and Vomvoris* [1983], *Snodgrass and Kitanidis* [1997], and *Michalak and Kitanidis* [2004a] for additional details.

[15] Inverse methods use modeling and statistical tools to determine the historical distribution of observed contamination, the location of contaminant sources, or the release history from a known source. The inverse problem is often underdetermined and an infinite number of parameters that are consistent with the data may be obtained [*Woodbury and Ulrych*, 1996]. *Kabala and Skaggs* [1998] stress that this nonuniqueness of the solution is caused by the ill-posed nature of the physical problem and is not associated with any particular solution methodology, nor can nonuniqueness be eliminated with any particular procedure. Indeed, there are numerous inverse modeling methods; see, for example, reviews by *Michalak and Kitanidis* [2004a] and *Atmadja and Bagtzoglou* [2001]. Of the available methods, only those that provide a stochastic solution to the problem of source estimation can potentially be applied to improve plume estimation, because the uncertainty of the loading history needs to be quantified in order to, in turn, determine the precision with which the plume distribution can be

estimated. Backward tracking [*Bagtzoglou et al.*, 1991, 1992] and adjoint-derived source distribution probabilities [*Neupauer and Wilson*, 2001] are two available stochastic approaches, but these methods are only applicable to identifying the location or release time of a single instantaneous point source. The geostatistical approach to inverse modeling [*Snodgrass and Kitanidis*, 1997; *Michalak and Kitanidis*, 2003, 2004a, 2004b, 2005; *Butera and Tanda*, 2003] and the minimum relative entropy method [*Woodbury and Ulrych*, 1996, 1998], conversely, are stochastic methods that provide a function estimate to characterize the historical contaminant distribution, source location, or release history. For these methods, the contaminant distribution or source description is not limited to a small set number of fixed parameters but can instead vary in space and/or in time. The applicability of the geostatistical method has already been demonstrated for multidimensional heterogeneous media [*Michalak and Kitanidis*, 2004a] and is similar in form to geostatistical kriging. The stochastic nature of the geostatistical approach to inverse modeling, which allows the uncertainty of the estimate to be quantified, and its affinity to kriging, which allows for a convenient setup of a familiar equation system, make it an appropriate basis for the proposed plume estimation methods.

[16] The geostatistical approach to inverse modeling is based on the dual criterion of reproducing available concentration data $\mathbf{z}^*$ and preserving spatial or temporal autocorrelation in some unknown function $\mathbf{s}[m \times 1]$, such as the release history of contaminants into the aquifer. The method begins by calculating the sensitivity of available concentration measurements to the unknown function, and assigning this information to a Jacobian matrix $\mathbf{H}^*$ (i.e., $H^*_{ij} = \partial z^*_i / \partial s_j$). This sensitivity information is then used in combination with the available data and their associated uncertainty to estimate a discretized version of the unknown function. This unknown function is assumed to be spatially and/or temporally autocorrelated.

[17] This form of inverse modeling relies on the existence of a groundwater flow and contaminant transport model. This usually implies knowledge of parameters such as the hydraulic conductivity field, the dispersivity tensor, the boundary conditions, etc. In addition, the transport model must either be linear or meet certain conditions which would enable a quasi-linear approximation (see *Kitanidis* [1996] for details). In this work, as in past applications of the geostatistical approach to inverse modeling for contaminant source identification [e.g., *Snodgrass and Kitanidis*, 1997; *Michalak and Kitanidis*, 2002, 2003, 2004a, 2004b], the transport model itself is assumed to be deterministically known. The concentrations of the source and of the measurements, on the other hand, are treated as random functions in a geostatistical framework.

[18] The transport model is sampled at measurement locations and times to yield a sensitivity matrix. If we are estimating the source release history on the basis of concentrations measured in the plume at a single time but at different locations, each element H^*_{ij} of this sensitivity matrix represents the sensitivity of the concentration at location x^*_i $[i = 1..\ n]$ to the source intensity at time t_j $[j = 1..\ m]$. The product of this sensitivity matrix and a temporal source function $\mathbf{s}$ reproduces the measured concentrations $\mathbf{z}^*$ at all locations x^*_i, to within a model-data mismatch error ϵ:

$$\mathbf{z}^* = \mathbf{H}^*\mathbf{s} + \epsilon \tag{1}$$

where ϵ is assumed to be a zero-mean model-data mismatch error with covariance matrix $\mathbf{R}$. Because measurement errors are usually not correlated in space and typically have a uniform variance σ^2_R, the covariance structure is modeled as $\mathbf{R} = \sigma^2_R\mathbf{I}$, where $\mathbf{I}$ is an $[n \times n]$ identity matrix. σ^2_R can either be known a priori, or estimated from available data (see below). Note that the model-data mismatch can also include transport error or microvariability not explained by the model. Thus, even though the model is deterministic, some forms of transport model uncertainties can be taken into account.

[19] The expected value of $\mathbf{s}$ is modeled as $E[\mathbf{s}] = \mathbf{X}_s\boldsymbol{\beta}_s$, where $\mathbf{X}_s$ is a known $[m \times p_s]$ matrix of basis functions and $\boldsymbol{\beta}_s$ are p_s unknown drift coefficients. The prior covariance function of $\mathbf{s}$ is a known function $\mathbf{Q}_s(\boldsymbol{\theta}) = E[(\mathbf{s} - \mathbf{X}_s\boldsymbol{\beta}_s)(\mathbf{s} - \mathbf{X}_s\boldsymbol{\beta}_s)^T]$ of unknown parameters $\boldsymbol{\theta}$, which can be estimated, for example, using a restricted maximum likelihood (RML) approach [*Kitanidis*, 1995]. This approach minimizes the negative log likelihood of the probability of the measurements with respect to the covariance parameters $\boldsymbol{\theta}$:

$$L_{\boldsymbol{\theta}} = \frac{1}{2}\ln|\Sigma| + \frac{1}{2}\ln\left|\mathbf{X}_s^T\mathbf{H}^{*T}\boldsymbol{\Sigma}^{-1}\mathbf{H}^*\mathbf{X}_s\right| + \frac{1}{2}\mathbf{z}^{*T}\boldsymbol{\Xi}\mathbf{z}^* \tag{2}$$

where $\boldsymbol{\Sigma} = \mathbf{H}^*\mathbf{Q}_s\mathbf{H}^{*T} + \mathbf{R}$ and

$$\boldsymbol{\Xi} = \boldsymbol{\Sigma}^{-1} - \boldsymbol{\Sigma}^{-1}\mathbf{H}^*\mathbf{X}_s\left(\mathbf{X}_s^T\mathbf{H}^{*T}\boldsymbol{\Sigma}^{-1}\mathbf{H}^*\mathbf{X}_s\right)^{-1}\mathbf{X}_s^T\mathbf{H}^{*T}\boldsymbol{\Sigma}^{-1} \tag{3}$$

In addition to the parameters in $\mathbf{Q}_s$, the variance of the model-data mismatch errors σ^2_R can also be estimated as part of this system.

[20] Once the covariance parameters $\boldsymbol{\theta}$ have been optimized, the source is estimated by minimizing:

$$L_{\mathbf{s},\boldsymbol{\beta}_s} = \frac{1}{2}(\mathbf{z}^* - \mathbf{H}^*\mathbf{s})^T\mathbf{R}^{-1}(\mathbf{z}^* - \mathbf{H}^*\mathbf{s}) + \frac{1}{2}(\mathbf{s} - \mathbf{X}_s\boldsymbol{\beta}_s)^T\mathbf{Q}_s^{-1}(\mathbf{s} - \mathbf{X}_s\boldsymbol{\beta}_s) \tag{4}$$

which can be expressed as the following system of $[n + p_s]$ equations

$$\begin{bmatrix} \mathbf{H}^*\mathbf{Q}_s\mathbf{H}^{*T} + \mathbf{R} & \mathbf{H}^*\mathbf{X}_s \\ (\mathbf{H}^*\mathbf{X}_s)^T & \mathbf{0} \end{bmatrix} \begin{bmatrix} \boldsymbol{\Lambda}_s^T \\ \mathbf{M}_s \end{bmatrix} = \begin{bmatrix} \mathbf{H}^*\mathbf{Q}_s \\ \mathbf{X}_s^T \end{bmatrix} \tag{5}$$

This system is solved for the $[m \times n]$ matrix of coefficients $\boldsymbol{\Lambda}_s$ and the $[p_s \times m]$ matrix of Lagrange multipliers $\mathbf{M}_s$, from which the best estimate and posterior covariance of the source function can be found:

$$\hat{\mathbf{s}} = \boldsymbol{\Lambda}_s\mathbf{z}^* \tag{6}$$

$$\mathbf{V}_{\hat{\mathbf{s}}} = \mathbf{Q}_s - \mathbf{Q}_s\mathbf{H}^{*T}\boldsymbol{\Lambda}_s^T - \mathbf{X}_s\mathbf{M}_s \tag{7}$$

4.2. Proposed Methods

4.2.1. Inverse/Forward Modeling

[21] In the IFM approach, the contaminant release history estimated using geostatistical inverse modeling is used to obtain an estimate of the distribution of the plume at the time of sampling, and its associated uncertainty. The contaminant plume is reconstructed by simulating transport of the estimated release history up to the measurement time(s). This step involves calculating an expanded sensitivity matrix $\mathbf{H}$ [$N \times m$] which defines the sensitivity of N locations in the aquifer at the time when the measurements were taken to the m discretized times of the contaminant release history. The elements of $\mathbf{H}$ can be obtained numerically by running the groundwater transport model with unit releases of contaminant for each time t_j [$j = 1..\ m$] and recording the resulting concentration at each of the N locations where the plume concentration is to be estimated. Typically, these N points would be laid out on a regular grid, to allow for easy contouring of the estimated plume distribution. The best estimate of the concentrations is estimated using the resulting linear model

$$\hat{\mathbf{z}} = \mathbf{H}\hat{\mathbf{s}} \tag{8}$$

where $\hat{\mathbf{z}}$ are the [$N \times 1$] estimates of the concentrations $\mathbf{z}$. Note that we use $\mathbf{z}^*$ to designate concentration at measurement locations, and $\mathbf{z}$ to designate the concentrations that we are interested in estimating. The same sensitivity matrix $\mathbf{H}$ can also be used to define the uncertainty and covariance of the estimated plume distribution, which is a function of the uncertainty associated with the recovered contaminant release history:

$$\mathbf{V}_{\hat{\mathbf{z}}} = \mathbf{H}\mathbf{V}_{\hat{\mathbf{s}}}\mathbf{H}^T \tag{9}$$

The diagonal elements of this [$N \times N$] matrix represent the uncertainty of the estimated concentration spatial distribution.

4.2.2. Transport-Enhanced Kriging

[22] The second plume estimation method also relies on the estimated release history (equation (6)) but also takes into account the spatial covariance $\mathbf{Q}_z$ of the plume concentration distribution, where $\mathbf{Q}_z(\boldsymbol{\theta}) = E[(\mathbf{z} - \mathbf{X}_z\boldsymbol{\beta}_z)(\mathbf{z} - \mathbf{X}_z\boldsymbol{\beta}_z)^T]$, and $E[\mathbf{z}] = \mathbf{X}_z\boldsymbol{\beta}_z$. This covariance can also be estimated using the subset of available concentration values $\mathbf{z}^*$ using an RML approach, with the objective function simplifying to:

$$L_{\boldsymbol{\theta}} = \frac{1}{2}\ln|\mathbf{Q}^*_{z^*}| + \frac{1}{2}\ln\left|\mathbf{X}_z^{*T}\mathbf{Q}_{z^*}^{*-1}\mathbf{X}_z^*\right| + \frac{1}{2}\mathbf{z}^{*T}\left(\mathbf{Q}_{z^*}^{*-1} - \mathbf{Q}_{z^*}^{*-1}\mathbf{X}_z^*\left(\mathbf{X}_z^{*T}\mathbf{Q}_{z^*}^{*-1}\mathbf{X}_z^*\right)^{-1}\mathbf{X}_z^{*T}\mathbf{Q}_{z^*}^{*-1}\right)\mathbf{z}^* \tag{10}$$

where the basis functions $\mathbf{X}_z^*$ [$n \times p_z$] and covariance model $\mathbf{Q}^*_{z^*}$ [$n \times n$] are the same as $\mathbf{X}_z$ and $\mathbf{Q}_z$, but are only evaluated at the measurement locations. This correlation in deviations of the concentration distribution from its underlying trend $\mathbf{X}_z\boldsymbol{\beta}_z$ may provide information not available through the transport model alone. In assimilating the covariance information $\mathbf{Q}_z$, we simultaneously require that the covariance structure imposed by the physical transport model and that implied by the spatial autocorrelation of the measurements are honored. Explicitly, the residuals between the model predictions $\mathbf{H}\hat{\mathbf{s}}$ and the TREK estimates $\hat{\mathbf{z}}$ should be consistent with the covariance structure implied by the uncertainty of the release history and by the transport model, i.e., $\mathbf{H}\mathbf{V}_{\hat{\mathbf{s}}}\mathbf{H}^T$. In addition, the residuals from the measurement-space trend $\mathbf{X}_z\boldsymbol{\beta}_z$ should have the spatial structure $\mathbf{Q}_z$. These requirements are assimilated in a second Bayesian step, minimizing:

$$L_{\mathbf{z},\boldsymbol{\beta}_z} = \frac{1}{2}(\mathbf{H}\hat{\mathbf{s}} - \mathbf{z})^T\left(\mathbf{H}\mathbf{V}_{\hat{\mathbf{s}}}\mathbf{H}^T\right)^{-1}(\mathbf{H}\hat{\mathbf{s}} - \mathbf{z}) + \frac{1}{2}(\mathbf{z} - \mathbf{X}_z\boldsymbol{\beta}_z)^T\mathbf{Q}_z^{-1}(\mathbf{z} - \mathbf{X}_z\boldsymbol{\beta}_z) \tag{11}$$

with respect to the unknown concentrations $\mathbf{z}$ [$N \times 1$] and the p_z spatial drift parameters $\boldsymbol{\beta}_z$. The first term in this objective function makes use of the inverse modeling best estimate $\hat{\mathbf{s}}$ and its posterior covariance, whereas the second term requires the estimates to follow the kriging trend $\mathbf{X}_z\boldsymbol{\beta}_z$ and covariance $\mathbf{Q}_z$. Note that the measured concentration values $\mathbf{z}^*$ do not reappear in this second objective function. The second system of equations to be solved becomes:

$$\begin{bmatrix} \mathbf{Q}_z + \mathbf{H}\mathbf{V}_{\hat{\mathbf{s}}}\mathbf{H}^T & \mathbf{X}_z \\ \mathbf{X}_z^T & \mathbf{0} \end{bmatrix}\begin{bmatrix} \boldsymbol{\Lambda}_z^T \\ \mathbf{M}_z \end{bmatrix} = \begin{bmatrix} \mathbf{Q}_z \\ \mathbf{X}_z^T \end{bmatrix} \tag{12}$$

Note that these $(N + p_z)$ equations can be set up only after the inverse modeling system has been solved for $\hat{\mathbf{s}}$ and for $\mathbf{V}_{\hat{\mathbf{s}}}$. The solutions of this system, $\boldsymbol{\Lambda}_z$ [$N \times N$] and $\mathbf{M}_z$ [$p_z \times N$], are used to compute the plume concentration distribution and its covariance:

$$\hat{\mathbf{z}} = \boldsymbol{\Lambda}_z\mathbf{H}\hat{\mathbf{s}} \tag{13}$$

$$\mathbf{V}_{\hat{\mathbf{z}}} = \mathbf{Q}_z - \mathbf{Q}_z\boldsymbol{\Lambda}_z^T - \mathbf{X}_z\mathbf{M}_z \tag{14}$$

Here $\hat{\mathbf{z}}$ is the TREK best estimate of the plume distribution, and $\mathbf{V}_{\hat{\mathbf{z}}}$ is the corresponding covariance structure.

4.2.3. Uncertainties Modeled in IFM and TREK

[23] For geostatistical inverse modeling, the matrix $\mathbf{V}_{\hat{\mathbf{s}}}$ represents the covariance of the a posteriori source function residuals ($\mathbf{s} - \hat{\mathbf{s}}$), and its diagonal elements correspond to the uncertainty of the best estimate $\hat{\mathbf{s}}$. For IFM, $\mathbf{V}_{\hat{\mathbf{s}}}$ is used to define the covariance of the full plume concentration distribution, using the model matrix $\mathbf{H}$ to yield $\mathbf{H}\mathbf{V}_{\hat{\mathbf{s}}}\mathbf{H}^T$. Thus, for a given model $\mathbf{H}$, the uncertainty of an estimate at a given point depends on its sensitivity to the source function. For example, the sensitivity will be greater for regions immediately downgradient from the source, while areas further downgradient or away from the principal flow direction are much less sensitive to the release intensity. The result is that the uncertainty will decrease, in general, with growing distance from the contamination source. The uncertainty also depends on $\mathbf{V}_{\hat{\mathbf{s}}}$ such that plume areas corresponding to times at which the release was highly uncertain will have higher variance than those corresponding to more certain elements of $\mathbf{s}$.

[24] Similar considerations determine the uncertainty associated with TREK estimates, because this method also relies on the estimated release history. However, TREK may

be more directly affected by measurement locations, since it also considers the spatial covariance structure of the plume distribution, $\mathbf{Q}_z$. This additional information further constrains the estimate for each point, with the result that the TREK uncertainty is always smaller than that of IFM.

4.3. Kriging With a Trend

[25] The new methods presented in section 4.2 are compared to kriging in the applications presented in section 5. Therefore a brief overview of kriging is presented here for reference. In kriging with a trend, we model $\mathbf{z}$ as a random vector with expected value $\mathbf{X}_z\boldsymbol{\beta}_z$, where $\mathbf{X}_z$ is a known $[N \times p_z]$ matrix and $\boldsymbol{\beta}_z$ are p_z unknown drift coefficients, representing the mean and the trend of the unknown concentration distribution. The prior covariance of $\mathbf{z}$ is $\mathbf{Q}_z$, a known function of unknown parameter(s) $\boldsymbol{\theta}$, which can be optimized using RML as presented in Section 4.2. Once these parameters have been estimated, the best estimate $\hat{\mathbf{z}}$ is obtained using a linear combination of known measurements $\mathbf{z}^*$. The coefficients $\boldsymbol{\Lambda}_{z*}$ $[N \times n]$ and $\mathbf{M}_{z*}$ $[p_z \times N]$ of this linear system are calculated by solving a kriging system of the form

$$\begin{bmatrix} \mathbf{Q}^*_{z*} & \mathbf{X}^*_z \\ \mathbf{X}^{*T}_z & \mathbf{0} \end{bmatrix} \begin{bmatrix} \boldsymbol{\Lambda}^T_{z*} \\ \mathbf{M}_{z*} \end{bmatrix} = \begin{bmatrix} \mathbf{Q}_{z*} \\ \mathbf{X}^T_z \end{bmatrix} \tag{15}$$

Note that $\mathbf{Q}^*_{z*}$ $[n \times n]$ is the covariance matrix of measurements, whereas $\mathbf{Q}_{z*}$ $[n \times N]$ is the covariance between concentrations at the n measurements locations and the N estimation locations. Similarly, $\mathbf{X}^*_z$ are the basis functions evaluated at the measurement locations, and $\mathbf{X}_z$ are those evaluated at the estimation locations. The kriging estimator is

$$\hat{\mathbf{z}} = \boldsymbol{\Lambda}_{z*}\mathbf{z}^* \tag{16}$$

and the a posteriori kriging covariance is

$$\mathbf{V}_{\hat{\mathbf{z}}} = \mathbf{Q}_z - \mathbf{Q}^T_{z*}\boldsymbol{\Lambda}^T_{z*} - \mathbf{X}_z\mathbf{M}_{z*} \tag{17}$$

[26] To account for measurement errors and preserve continuity, continuous part kriging [*Kitanidis*, 1997], also referred to as kriging with known measurement error variance [*Wackernagel*, 2003], can be applied by adding σ^2_R to the terms on the diagonal of $\mathbf{Q}^*_{z*}$ in equation (15).

5. Test Cases

[27] The following section presents sample applications of the two methods developed in this work. These examples involve the estimation of a contaminant plume distribution in a confined aquifer. In all examples, an aquifer is assumed to have been contaminated by a single point source with known location but unknown loading history as a function of time, $\mathbf{s}$. Measurements $\mathbf{z}^*$ taken at time T and knowledge of the hydrogeological conditions, $\mathbf{H}$ and $\mathbf{H}^*$, are used in implementing IFM, TREK, and KT, to estimate the full plume distributions $\mathbf{z}$. Hypothetical examples were chosen to illustrate and verify the capabilities of the methods in a setup where the true concentration distributions are known.

[28] The two cases considered are a plume in a one-dimensional homogeneous aquifer, and a plume in a two-dimensional heterogeneous aquifer. In addition, sensitivity analyses are performed to evaluate the effects of monitoring network configurations, measurement errors, the time elapsed prior to sampling, and spatially correlated model mismatch errors.

5.1. Example 1: One-Dimensional Homogeneous Aquifer

[29] In the first example we use the setup previously implemented by *Skaggs and Kabala* [1994, 1995] and *Snodgrass and Kitanidis* [1997]. This example involves the release of a conservative solute into a one-dimensional homogeneous aquifer with a steady state flow field. The solute is released only at the origin ($x_0 = 0$) and the concentration is measured at various points in the aquifer at some later time T. The advective and dispersive transport of this solute can be expressed analytically as:

$$C(x,T) = \int_0^T s(t)g_{1D}(x, T-t)dt \tag{18}$$

where $C(x, T)$ is the concentration at distance x from the source and time T. The source is a function of time and is expressed by $s(t)$. The one-dimensional transfer function $g_{1D}(x, T-t)$ relates the source concentration at time t to the concentration measured at point x and time T [*Skaggs and Kabala*, 1994]:

$$g_{1D}(x,T-t) = \frac{x}{2\sqrt{\pi D_L (T-t)^3}} \exp\left[-\frac{(x-v(T-t))^2}{4D_L(T-t)}\right] \tag{19}$$

where D_L is the longitudinal dispersion coefficient and v is the seepage velocity. Note that $z_i = C(x_i, T)$ is the concentration at location x_i.

[30] The synthetic pollution event is obtained through the numerical integration of equation (18) at $T = 330$ time units, with longitudinal dispersivity $D_L = 1$, flow velocity $v = 1$ and true release history

$$s(t) = \exp\left[-\frac{(t-130)^2}{50}\right] + 0.3\exp\left[-\frac{(t-150)^2}{200}\right] + 0.5\exp\left[-\frac{(t-190)^2}{98}\right] \tag{20}$$

This release history is illustrated in Figure 1. Note that this release history is used only for the purposes of simulating the plume, but is then considered unknown in subsequent steps. This one-dimensional plume is sampled at $n = 11$ locations $\mathbf{x}^*$. Negligible measurement error with a variance of 10^{-12} is added to these concentrations to yield the observations $\mathbf{z}^*$. We use these observations $\mathbf{z}^*$ and the transport information (equation (19)) to estimate the plume concentrations $\mathbf{z}$ at $m = 301$ locations ($x = 0, 1, 2, \ldots, 300$) using KT, IFM and TREK.

5.1.1. Kriging With a Trend

[31] For kriging with a trend we use a cubic generalized covariance function (GCF):

$$\mathbf{Q}_z(h) = \theta_z h^3 \tag{21}$$

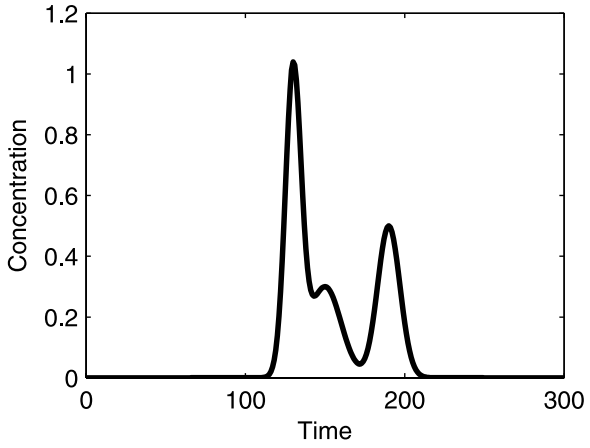

Figure 1. Example 1: Source release history.

and optimize the parameter θ_z using RML. In order to obtain better structural information, we use more plume samples for this optimization step than for the estimation below. For this example, the estimated parameter is $\theta_z = 5.9 \times 10^{-8}$.

[32] The plume is modeled using a linear trend in x, yielding $\mathbf{X}_z^* = [[\mathbf{1}]\ \mathbf{x}^*]$, where $[\mathbf{1}]$ is an $(n \times 1)$ vector of ones. The coefficients $\mathbf{\Lambda}_{z*}$ and $\mathbf{M}_{z*}$, calculated with equation (15), are used to obtain the best estimate $\hat{\mathbf{z}}$ (equation (16)) of the plume distribution and the kriging covariance $\mathbf{V}_{\hat{\mathbf{z}}}$ (equation (17)). Measurement The best estimate and associated uncertainty are plotted in Figure 2.

5.1.2. Inverse/Forward Modeling

[33] We use the transfer function (equation (19)) to define the sensitivity matrix $\mathbf{H}^*$ according to [*Snodgrass and Kitanidis*, 1997]

$$H_{ij}^* = \frac{x_i^*}{2\sqrt{\pi D_L (T - t_j)^3}} \exp\left[-\frac{(x_i^* - v(T - t_j))^2}{4D_L(T - t_j)}\right] \Delta t \qquad (22)$$

where $\Delta t = 1$ is the discretization of the source function in time. The covariance structure $\mathbf{Q}_s$ of the source function is also modeled using a cubic GCF. For the presented example, the best estimate for its single parameter (optimized using RML) is $\theta_s = 1.3 \times 10^{-5}$. This information is used to estimate the source release history (equations (5), (6), and (7)). The source function basis functions are $\mathbf{X}_s = [[\mathbf{1}]\ \mathbf{t}]$, where $[\mathbf{1}]$ is an $[m \times 1]$ vector of ones and the elements of $\mathbf{t} = 0, 1, \ldots, 300$ correspond to the discretized times of the release history. We then form a second sensitivity matrix $\mathbf{H}$ for the estimation points $\mathbf{x}$, by replacing the measurement locations x_i^* with estimation locations x_i in equation (22). The resulting estimated plume distribution $\hat{\mathbf{z}}$ and its covariance $\mathbf{H}\mathbf{V}_{\hat{\mathbf{s}}}\mathbf{H}^T$ are illustrated in Figure 2.

[34] The IFM best estimate fluctuates around the actual plume while reproducing all of the measurements to within the prescribed measurement error. The plume samples were

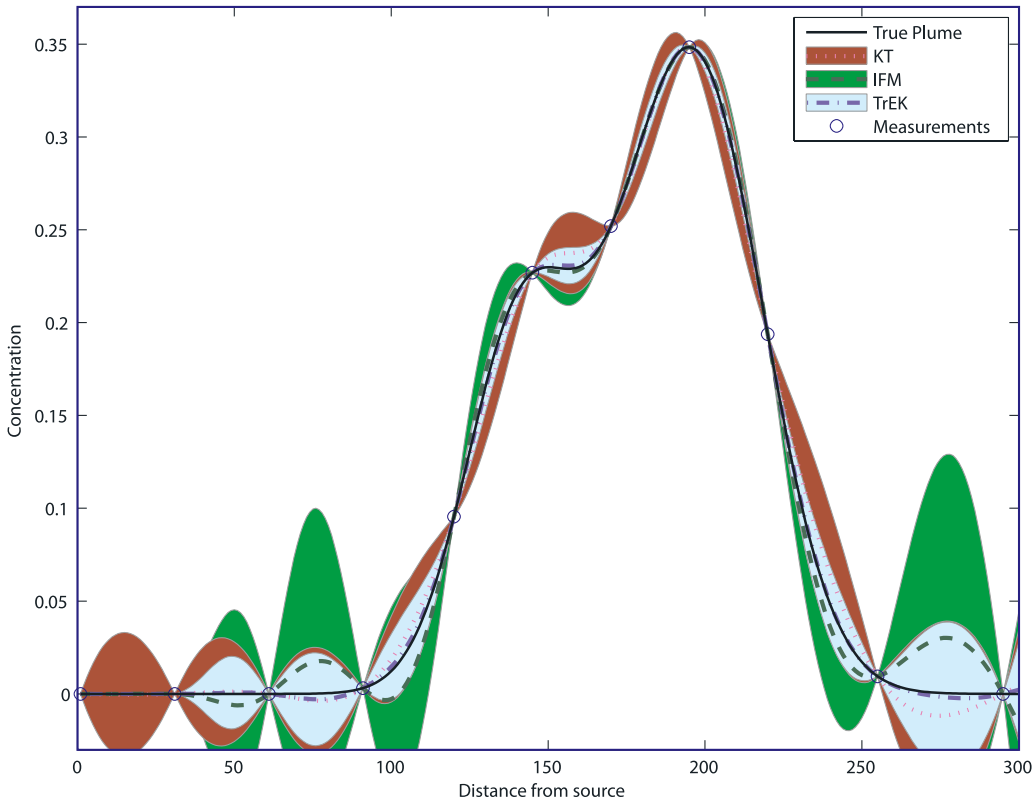

Figure 2. Example 1: Homogeneous one-dimensional plume. Lines represent best estimates; shaded areas represent 95% confidence intervals.

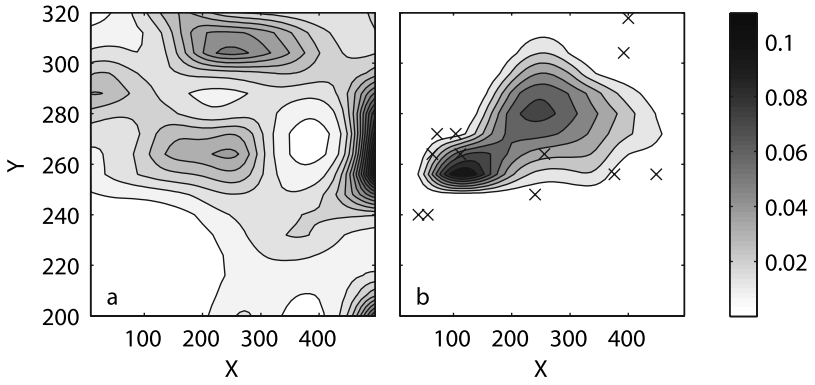

Figure 3. Example 2: Heterogeneous two-dimensional aquifer. (a) Hydraulic conductivity field. (b) Simulated plume and measurement locations. All quantities are dimensionless.

all taken 30 time units after the modeled contamination event ceased; however, the constant flow remained as before. Consequently, uncontaminated water flowed in from the left side of the aquifer. Thus a significant concentration around $x \approx 0$ is physically nearly impossible according to the transport model. For this reason, IFM's confidence intervals vanish there.

5.1.3. Transport-Enhanced Kriging

[35] In this third approach, we estimate the release history of the point source as described in section 4.3. We then use the concentration covariance structure $\mathbf{Q}_z$ together with the inverse modeling results to estimate the plume distribution according to equations (12)–(14). Results are presented in Figure 2.

[36] With 11 available measurements, and no significant measurement error ($\sigma_R = 10^{-6}$), all three methods do reasonably well in reproducing the true (unknown) concentration distribution throughout the domain. At several points, the KT and IFM curves deviate noticeably from the actual plume, whereas the TREK estimates remain closest to the actual distribution. The confidence intervals show that uncertainty decreases close to measurement locations for all methods. For any given point, the transport-enhanced kriging (TREK) has the lowest uncertainty because it combines the information used in KT and IFM. All methods yield reasonable estimates of uncertainty, in the sense that the real plume falls within the 95% confidence intervals in most areas. However, the TREK estimate yields the most accurate representation of the true plume distribution.

5.2. Example 2: Two-Dimensional Heterogeneous Aquifer

[37] In this example, a contaminant is released into a deterministically heterogeneous confined aquifer (Figure 3a). The concentration of the point source located at ($x_1 = 0$, $y_1 = 260$) is variable in time and is described by

$$s(t) = 1.4 \exp\left[-\frac{(t-850)^2}{56000}\right] + 1.1 \exp\left[-\frac{(t-1700)^2}{13333}\right] \quad (23)$$

The resulting plume is measured at $n = 12$ locations (Figure 3b), to yield the observations $\mathbf{z}^*$. A normally distributed random error, with a variance of $\sigma_R^2 = 10^{-6}$, was added to these measurements.

[38] The conductivity field for this aquifer is taken from *Michalak and Kitanidis* [2004a]. A constant head difference was imposed between the left and right boundaries of the aquifer, inducing flow from left to right. On the top and bottom are zero-flux (no flow) boundaries. MODFLOW-2000 [*Hill et al.*, 2000] is used to calculate the corresponding flow field.

[39] The numerical transport model MT3DMS [*Zheng and Wang*, 1999] is used in implementing IFM and TREK to determine the effect of a unit concentration pulse on field concentrations. A short pulse is released, and the resultant concentrations are sampled repeatedly on a grid of 16×62 locations, at 188 consecutive times, corresponding to the discretization of the source release history $\mathbf{s}$. Thus, although the transport model is run only once, it effectively yields the required sensitivities for all times of the release history. The concentrations measured at each time step are used to fill one column of the sensitivity matrix $\mathbf{H}$.

[40] We use a typical 10:1 anisotropy [e.g., *Delleur*, 1998] for the kriging estimation, corresponding to the modeled ratio of longitudinal (0.347) to transverse dispersivity (0.0347). Note that only the ratio of the dispersivity values is needed to define the kriging anisotropy [*Chilès and Delfiner*, 1999]. Using the measurements $\mathbf{z}^*$, covariance parameters are optimized both for the source function and for the measurement space using cubic GCFs, yielding $\theta_s = 1.3 \times 10^{-8}$ and $\theta_z = 1.4 \times 10^{-9}$, respectively. Note that θ_z is estimated in a transformed coordinate system, in which the y coordinate was stretched to account for anisotropy.

[41] As in the previous example, KT, IFM and TREK are used to estimate the simulated plume. The KT interpolation (Figure 4a) reproduces the measurements, but is unable to represent the true shape of the plume, and its uncertainty (Figure 4d) grows quickly away from measurement locations. The IFM method reproduces the plume much more precisely (Figure 4b), and yields a substantially lower uncertainty (Figure 4e). Contrary to KT, the uncertainty decreases with increasing distance from the center of the plume. Finally, the TREK solution (Figure 4c) is very similar to the IFM solution, but slightly better. The uncertainty is always lowest relative to KT and IFM.

[42] Figure 5 shows the recovered source function (equation (6)) for this example and its confidence intervals (equation (7)). With only 12 concentration measurements,

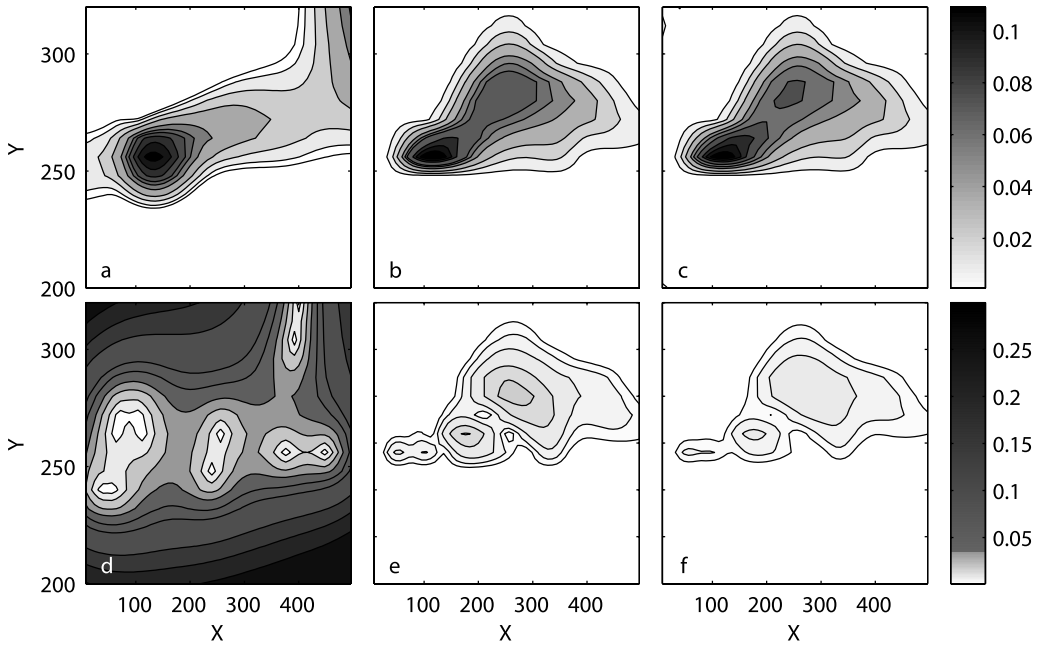

Figure 4. Example 2: Results. (a) Kriging with a trend best estimate. (b) Inverse/forward modeling best estimate. (c) Transport-enhanced kriging best estimate. (d) Kriging with a trend uncertainty. (e) Inverse/forward modeling uncertainty. (f) Transport-enhanced kriging uncertainty. All quantities are dimensionless; uncertainties are represented by standard deviation.

the best estimate of the release history differs from the true loading substantially, and the uncertainty associated with the estimate is large. This demonstrates the strongly underdetermined nature of this inverse problem (12 data points are used to estimate the 188 points of the source function). Note that the estimated source release history is still accurate because the true function lies within the uncertainty bounds of the estimate. Most interestingly, however, even with a poor estimate for the source function, the IFM and TREK methods reproduce the true plume very well (Figures 4b and 4c). This is due both to the fact that (1) the nature of the flow and transport in the aquifer provides a strong constraint on the possible plume distributions, and that (2) the forward problem of contaminant transport is a well-posed problem, such that the resulting plume distribution is unique for a given release history and relatively insensitive to small uncertainties in this release [*Sun*, 1994]. Therefore, even in cases where the measurement network is not sufficient to constrain the source release history, incorporating information on the flow and transport field leads to significant improvements in the ability to estimate the spatial distribution of the contaminant plume.

5.3. Sensitivity Analyses

[43] Sensitivity analyses were performed to investigate the effects of increased measurement errors, correlated model-data mismatch errors, and sparse sampling networks on the performance of the proposed methods. The sparse network example is also repeated for multiple times after the release, to draw conclusions about how the methods behave for plumes that have undergone different degrees of transport and mixing.

5.3.1. Measurement Errors

[44] In the first sensitivity test (Figure 6), we use a similar setup to that of example 1, but introduce a measurement error of $\sigma_R = 0.01$. The cubic GCF parameters become $\theta_s = 8.9 \times 10^{-6}$ and $\theta_z = 6.5 \times 10^{-8}$. The best estimates are now conditioned to imperfect measurements, rather than to the actual plume, where this error can represent instrument error and/or uncorrelated errors associated with the transport model. For this case, as expected, the confidence intervals are wider relative to the case with negligible measurement error, especially near the measurement locations. TREK again provides the most precise plume estimates.

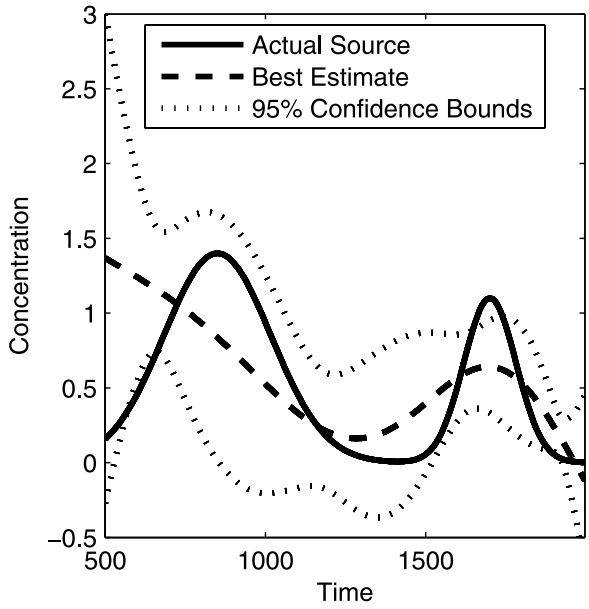

Figure 5. Example 2: Actual and estimated source release history.

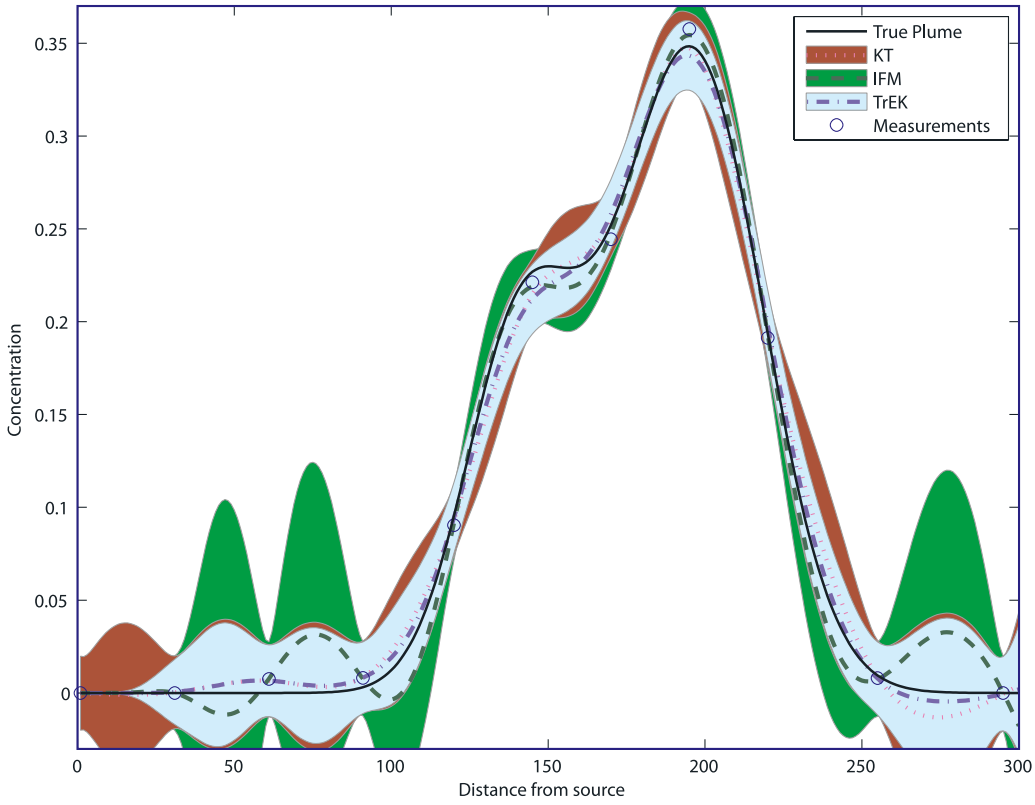

Figure 6. First sensitivity analysis: Example 1 with normally distributed measurement errors with standard deviation of 0.01.

5.3.2. Repeated Sampling in a Sparse Sampling Network

[45] We again use the setup described in example 1, but take measurements at only eight locations, to aggravate the ill posedness of the problem (now only 8 measurements are used to estimate 301 points). We sample this plume as it evolves over time. For T = 330 (Figure 7a), this sparse network results in poorer best estimates and wider confidence bounds for all methods. Note that the actual plume is still contained within the confidence bounds. At later times, T = 500 (Figure 7b) and T = 1500 (Figure 7c), the estimated plumes are closer to the actual plume, because the plume becomes smoother with time. This makes any kind of sparse network interpolation easier, because these methods tend by their nature to yield smooth estimates. For T = 500, the KT confidence intervals are similar to those for T = 330, but for IFM and TREK they decrease considerably. This occurs because the transport information yields more precise estimates as time lapses, because the effects of additional mixing mitigate the effects of the uncertain release history. At T = 1500, the plume is longer and the measurement network spans a larger area. Therefore the distance between adjacent measurement locations is larger, which increases the KT uncertainty. The IFM and TREK confidence intervals, on the other hand, are narrower owing to the degree of mixing implied by the flow and transport model. At large times, the actual plume becomes very smooth as a result of prolonged dispersion, and the three best estimates reproduce it very well and are almost indistinguishable (Figure 7c). At this large time, the accuracy of the kriging estimate is improved due to the smoothness of the plume, whereas the IFM and TREK estimates take advantage of this feature as well as the diffusive nature of the transport process.

5.3.3. Correlated Model-Data Mismatch Error

[46] If transport errors are present, then measurements cannot be reproduced perfectly, and this error is often parameterized as an additional measurement error. Recall that the first component of the inverse model objective function (equation (4)) requires the forward model **H*s** to reproduce the measurements **z*** to within an error with covariance **R**. Previously, this covariance matrix was modeled as a diagonal matrix, representing only independent measurement errors, with no cross-correlated errors. Nonzero off-diagonal terms in **R** imply that errors at certain points affect the values at other points. These effects can be interpreted as spatially correlated transport errors; hence we repeat example 2, replacing the uncorrelated **R** matrix with a cubic GCF with $\theta = 10^{-10}$, to investigate the effect of spatially correlated transport errors on the performance of IFM and TREK.

[47] Figure 8 shows the results of this sensitivity analysis. As expected, the best estimates are less precise than in experiment 2, yielding a smoother estimated plume distribution with higher uncertainty. The estimates remain accurate, however, providing a realistic estimate of the uncertainty associated with the plume distribution.

6. Discussion

[48] In the presented examples, the IFM and TREK methods are shown to be robust, providing good estimates

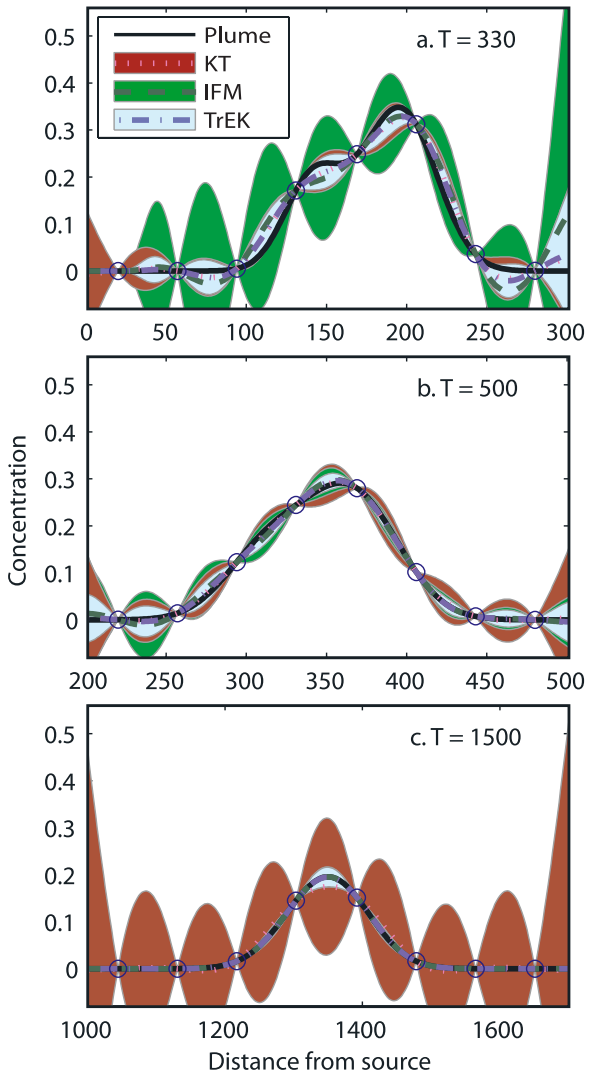

Figure 7. Second sensitivity analysis: Example 1 with sparse sampling network of eight equally spaced measurements at three different times. Note that the range of the abscissa is different in different subplots.

under a variety of conditions. Kriging with a trend, in contrast, is strongly dependent on measurement locations. The main reason behind this is that the new methods take advantage of transport information within the aquifer. IFM and TREK only allow solutions which are feasible in terms of the physical transport process. This is especially advantageous in heterogeneous formations (example 2), in which the measurement-based covariance function cannot capture small-scale variability. In KT, the estimate reverts to an estimated trend away from measurement locations. It is intuitive and well known that for KT and other direct interpolation methods, the uncertainty is lowest at the measurement locations, and increases with distance from them. In contrast, for IFM the highest uncertainties can sometimes be found directly downgradient from the source location (see example 2), because that is where any uncertainty in the recovered source release history has the most dramatic effect on concentrations. In the transverse direction, the contaminant concentration approaches zero with increasing distance, with little sensitivity to the source magnitude. The consequence is that if monitoring wells were to be drilled around the expected "hot spots" of the contamination, KT and IFM would complement each other: under certain circumstances, the former would have more precise predictions in areas of high concentrations, while the latter would more accurately predict the concentrations farther away. Thus careful implementation of the TREK method takes advantage of the best features of the other two approaches.

[49] Interestingly, although a sparse measurement network can lead to high uncertainty in the recovered contaminant release history, the process of forward modeling often mitigates this problem (Figure 5). This indicates that, although the sparse measurements are not sufficient to recover the source in some cases, the information provided by the flow and transport model provides an additional constraint that results in precise estimates of the current contaminant distribution. The flow regime in an aquifer and the contaminant source location provide a strong constraint on the possible distributions of plumes emanating from the source. In addition, groundwater contaminant transport is a dispersive process and consequently there are limits to what can be learned about the history of contamination from measurements of a plume's present spatial distribution [*Kabala and Skaggs*, 1998]. However, this dispersion is also the reason that the results of the forward model are relatively insensitive to the details of the release history, i.e., for a given transport model, large variations in the release would cause relatively smaller variations in the plume. Thus the additional constraint on the plume comes not only from the estimated release history, but also from the transport information itself. As a result, plumes can be estimated accurately even when the measurement network is not sufficient to strongly constrain the contaminant release history.

[50] The examples in this paper used deterministic transport models, with no inherent uncertainty. Other sources of uncertainty, such as the sparseness of the observation network, measurement errors, small-scale variations in concentrations, and model-data mismatch contributed to the uncertainty associated with the recovered source release history and plume distribution (Figures 2, 6, and 7a). In field situations, incomplete characterization of the subsurface would lead to additional uncertainty in the flow and transport model. This uncertainty would need to be quantified and included in the IFM and TREK plume distribution estimates, such that the estimated plume reflected the information content of the available model and measurements. In this work, the uncertainty associated with the flow and transport model is included in the variance (or covariance in the third sensitivity analysis) specified in the model-data mismatch matrix **R**. Methods for explicitly quantifying and taking in account spatially and/or temporally correlated flow and transport errors are the subject of ongoing research.

7. Conclusions

[51] The methods presented in this paper combine geostatistical kriging and inverse modeling approaches in developing improved tools for estimating the spatial distribution of contaminant plumes. The methods reconstruct the plume accurately with low uncertainty. In addition, IFM and

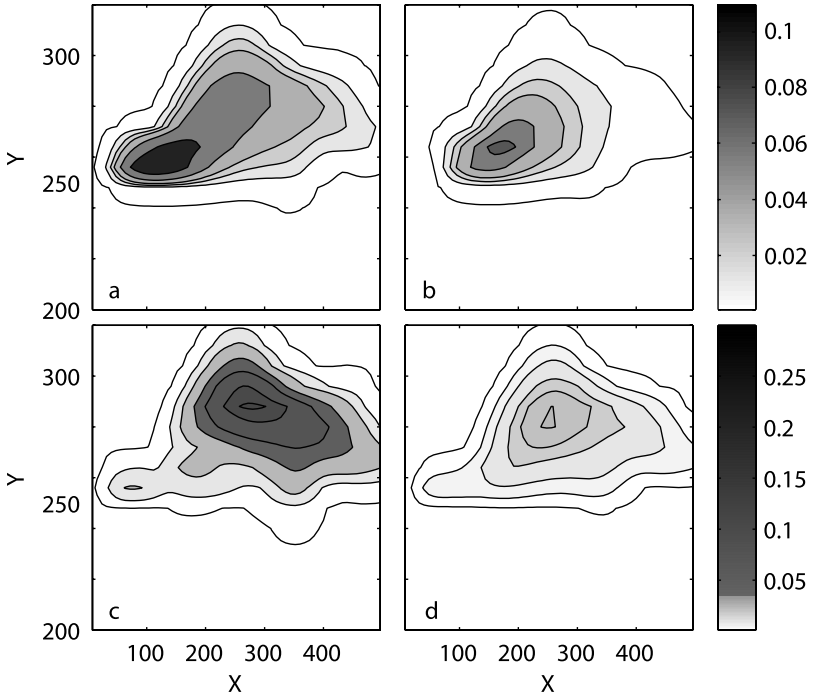

Figure 8. Third sensitivity analysis: Example 2 with spatially correlated model mismatch error matrix **R**. (a) Inverse/forward modeling best estimate. (b) Transport-enhanced kriging best estimate. (c) Inverse/forward modeling uncertainty. (d) Transport-enhanced kriging uncertainty. All quantities are dimensionless; uncertainties are represented by standard deviation.

TREK can often alleviate the effects of measurement errors by using transport information to eliminate values that are not physically feasible. The TREK method is most robust because it assimilates information about the transport as well as the spatial covariance structure of the measured concentrations. In cases where such a covariance structure is not available or not credible (e.g., measurements were taken in different hydrogeological zones), IFM would be the preferred choice.

[52] While the presented sample applications all assumed a single time-varying point source of contamination, the methods can easily be adapted to multiple point sources [e.g., *Butera and Tanda*, 2003], or to historical plume distributions [e.g. *Michalak and Kitanidis*, 2004a].

[53] It is interesting to note that, although we do not enforce nonnegativity in the estimated plume distribution, the IFM and TREK methods seldom yield estimates with negative concentrations, even though the estimated source function does sometimes exhibit negative concentrations. Nonnegativity-enforcing constraints could be explicitly imposed [e.g., *Snodgrass and Kitanidis*, 1997; *Michalak and Kitanidis*, 2003, 2005] to further improve plume interpolation using these methods. Such a modification would be expected to have a modest effect on the best estimates, but could have a more significant impact on the estimated uncertainty.

[54] We presented this work in a geostatistical framework, but the developed principles could potentially also be applied to other inversion methods. For example, the inversion of the release history could theoretically be performed using the minimum relative entropy approach [*Woodbury and Ulrych*, 1996], with the rest of the method unchanged, as long as the full covariance of the source release history were calculated.

[55] Finally, in the examples presented here, a deterministic transport field was used, and the location of the source was known. In field situations, these parameters may be uncertain, which would result in higher uncertainty in the estimated plume distribution, as demonstrated in the third sensitivity analysis. Future work will focus on incorporating these additional sources of uncertainty within the TREK framework to further enhance the applicability of this method in field situations.

[56] **Acknowledgments.** The authors would like to thank two anonymous reviewers for their helpful comments on this paper and Michael Fienen and Olaf Cirpka for valuable input on an earlier draft of this manuscript. The authors are also grateful to Alanood Alkhaled, Sharon Gourdji, Meng-Ying Li, and Kim Mueller for their input throughout the work on this paper. The Rackham Graduate School at the University of Michigan is gratefully acknowledged for providing a travel grant to Shahar Shlomi, which allowed preliminary findings of this work to be presented at the 2005 AGU Fall Meeting.

References

Atmadja, J., and A. C. Bagtzoglou (2001), State of the art report on mathematical methods for groundwater pollution source identification, *Environ. Forensics*, *2*, 205–214.

Bagtzoglou, A. C., et al. (1991), Probabilistic simulation for reliable solute source identification in heterogeneous porous media, in *Water Resources Engineering Risk Assessment*, *NATO ASI Ser., Ser. G*, vol. 29, pp. 189–201, Springer, New York.

Bagtzoglou, A. C., et al. (1992), Application of particle methods to reliable identification of groundwater pollution sources, *Water Resour. Manage.*, *6*, 15–23.

Boeckenhauer, R. K., et al. (2000), Statistical estimation and visualization of ground-water contamination data, *Rep. EPA/600/R-00/034*, U.S. Environ. Prot. Agency, Washington, D. C.

Butera, I., and M. G. Tanda (2003), A geostatistical approach to recover the release history of groundwater pollutants, *Water Resour. Res.*, *39*(12), 1372, doi:10.1029/2003WR002314.

Cassiani, G., and M. A. Medina (1997), Incorporating auxiliary geophysical data into ground-water estimation, *Ground Water*, *35*(1), 79–91.

Chilès, J.-P., and P. Delfiner (1999), *Geostatistics: Modeling Spatial Uncertainty*, John Wiley, Hoboken, N. J.

Commission on Geosciences, Environment and Resources (1993), *Ground Water Vulnerability Assessment: Predicting Relative Contamination Potential Under Conditions of Uncertainty*, Natl. Acad. Press, Washington, D. C.

Cooper, R. M., and J. D. Istok (1988), Geostatistics applied to groundwater contamination. 1. Methodology, *J. Environ. Eng.*, *114*(2), 270–286.

Delhomme, J. P. (1978), Kriging in the hydrosciences, *Adv. Water Resour.*, *1*, 251–266.

Delleur, J. W. (1998), *The Handbook of Groundwater Engineering*, CRC Press, Boca Raton, Fla.

Diggle, P. J., et al. (1998), Model-based geostatistics, *J. R. Stat. Soc., Ser. C*, *47*, 299–326.

Feehley, C. E., C. Zheng, and F. J. Molz (2000), A dual-domain mass transfer approach for modeling solute transport in heterogeneous aquifers: Application to the Macrodispersion Experiment (MADE) site, *Water Resour. Res.*, *36*, 2501–2515.

Figueira, R., et al. (2001), Use of secondary information in space-time statistics for biomonitoring studies of saline deposition, *Environmetrics*, *12*(3), 203–217.

Gomez-Hernanez, J. J., et al. (1997), Stochastic simulation of transmissivity fields conditional to both transmissivity and piezometric data—I. Theory, *J. Hydrol.*, *203*(1–4), 162–174.

Hill, M. C., et al. (2000), MODFLOW-2000, the U.S. Geological Survey modular ground-water model—User guide to modularization concepts and the ground-water flow process, *U.S. Geol. Surv. Techniques Methods*, *Book 6*, *Chap. A16*, 121 pp.

Jones, N. L., et al. (2003), A comparison of three-dimensional interpolation techniques for plume characterization, *Ground Water*, *41*(4), 411–419.

Journel, A. G., and C. V. Deutsch (1997), Rank order geostatistics: A proposal for a unique coding and common processing of diverse data, in *Geostatistics Wollongong '96*, pp. 174–187, Springer, New York.

Kabala, Z. J., and T. H. Skaggs (1998), Comment on ''Minimum relative entropy inversion: Theory and application to recovering the release history of a groundwater contaminant'' by Allan D. Woodbury and Tadeusz J. Ulrych, *Water Resour. Res.*, *34*, 2077–2079.

Kitanidis, P. K. (1995), Quasi-linear geostatistical theory for inversing, *Water Resour. Res.*, *31*, 2411–2419.

Kitanidis, P. K. (1996), On the geostatistical approach to the inverse problem, *Adv. Water Resour.*, *19*(6), 333–342.

Kitanidis, P. K. (1997), *Introduction to Geostatistics: Applications in Hydrogeology*, Cambridge Univ. Press, New York.

Kitanidis, P. K., and K. F. Shen (1996), Geostatistical interpolation of chemical concentration, *Adv. Water Resour.*, *19*(6), 369–378.

Kitanidis, P. K., and E. G. Vomvoris (1983), A geostatistical approach to the inverse problem in groundwater modeling (steady-state) and one-dimensional simulations, *Water Resour. Res.*, *19*, 677–690.

Liu, W. (2003), Development of gradient-enhanced kriging approximations for multidisciplinary design optimization, Ph.D. thesis, 177 pp., Univ. of Notre Dame, Notre Dame, Indiana.

Mackay, D. M., et al. (1986), A natural gradient experiment on solute transport in a sand aquifer: 1. Approach and overview of plume movement, *Water Resour. Res.*, *22*, 2017–2029.

Michalak, A. M., and P. K. Kitanidis (2002) Application of Bayesian inference methods to inverse modeling for contaminant source identification at Gloucester landfill, Canada, in *Computational Methods in Water Resources XIV*, vol. 2, edited by S. M. Hassanizadeh et al., pp. 1259–1266, Elsevier, New York.

Michalak, A. M., and P. K. Kitanidis (2003), A method for enforcing parameter nonnegativity in Bayesian inverse problems with an application to contaminant source identification, *Water Resour. Res.*, *39*(2), 1033, doi:10.1029/2002WR001480.

Michalak, A. M., and P. K. Kitanidis (2004a), Estimation of historical groundwater contaminant distribution using the adjoint state method applied to geostatistical inverse modeling, *Water Resour. Res.*, *40*, W08302, doi:10.1029/2004WR003214.

Michalak, A. M., and P. K. Kitanidis (2004b), Application of geostatistical inverse modeling to contaminant source identification at Dover AFB, Delaware, *J. Hydraul. Res.*, *42*(extra issue) 9–18.

Michalak, A. M., and P. K. Kitanidis (2005), A method for the interpolation of nonnegative functions with an application to contaminant load estimation, *Stochast. Environ. Res. Risk Assess.*, *19*(1), 8–23.

Neupauer, R. M., and J. L. Wilson (2001), Adjoint-derived location and travel time probabilities for a multidimensional groundwater system, *Water Resour. Res.*, *37*, 1657–1668.

Reed, P. M., et al. (2004), Spatial interpolation methods for nonstationary plume data, *Ground Water*, *42*(2), 190–202.

Saito, H., and P. Goovaerts (2001), Accounting for source location and transport direction into geostatistical prediction of contaminants, *Environ. Sci. Technol.*, *35*(24), 4823–4829.

Skaggs, T. H., and Z. J. Kabala (1994), Recovering the release history of a groundwater contaminant, *Water Resour. Res.*, *30*, 71–79.

Skaggs, T. H., and Z. J. Kabala (1995), Recovering the history of a groundwater contaminant plume: Method of quasi-reversibility, *Water Resour. Res.*, *31*, 2669–2673.

Snodgrass, M. F., and P. K. Kitanidis (1997), A geostatistical approach to contaminant source identification, *Water Resour. Res.*, *33*, 537–546.

Sun, N. Z. (1994), *Inverse Problems in Groundwater Modeling*, Springer, New York.

Vyas, V. M., et al. (2004), Geostatistical estimation of horizontal hydraulic conductivity for the Kirkwood-Cohansey aquifer, *J. Am. Water Resour. Assoc.*, *40*(1), 187–195.

Wackernagel, H. W. (2003), *Multivariate Geostatistics: An Introduction With Applications*, 3rd ed., Springer, New York.

Wagner, B. J., and S. M. Gorelick (1987), Optimal groundwater quality management under parameter uncertainty, *Water Resour. Res.*, *23*, 1162–1174.

Woodbury, A. D., and T. J. Ulrych (1996), Minimum relative entropy inversion: Theory and application to recovering the release history of a groundwater contaminant, *Water Resour. Res.*, *32*, 2671–2681.

Woodbury, A. D., and T. J. Ulrych (1998), Minimum relative entropy and probabilistic inversion in groundwater hydrology, *Stochast. Hydrol. Hydraul.*, *12*, 317–358.

Zheng, C. and P. P. Wang (1999), MT3DMS, a modular three-dimensional multi-species transport model for simulation of advection, dispersion and chemical reactions of contaminants in groundwater systems, documentation and user's guide, 202 pp., *Rep. SERDP-99-1 TA7 E8c*, U.S. Army Eng. Res. and Dev. Cent., Vicksburg, Miss.

A. M. Michalak and S. Shlomi, Department of Civil and Environmental Engineering, University of Michigan, EWRE Building, 1351 Beal Avenue, Ann Arbor, MI 48109-2125, USA. (anna.michalak@umich.edu; shaharsh@umich.edu)